J Ind Microbiol Biotechnol (2010) 37:1319–1326
DOI 10.1007/s10295-010-0876-5

ORIGINAL PAPER

Experimental validation of a nonequilibrium model of CO_2 fluxes between gas, liquid medium, and algae in a flat-panel photobioreactor

Ladislav Nedbal · Jan Červený · Nir Keren · Aaron Kaplan

Received: 10 July 2010 / Accepted: 13 September 2010

Abstract Carbon dioxide (CO_2) availability strongly affects the productivity of algal photobioreactors, where it is dynamically exchanged between different compartments, phases, and chemical forms. To understand the underlying processes, we constructed a nonequilibrium mathematical model of CO_2 dynamics in a flat-panel algal photobioreactor. The model includes mass transfer to the algal suspension from a stream of bubbles of CO_2-enriched air and from the photobioreactor headspace. Also included are the hydration of dissolved CO_2 to bicarbonate ion (HCO_3^-) as well as uptake and/or cycling of these two chemical forms by the cells. The model was validated in experiments using a laboratory-scale flat-panel photobioreactor that controls light, temperature, and pH and where the concentration of dissolved CO_2, and partial pressure of CO_2 in the photobioreactor exhaust are measured. First, the model prediction was compared with measured CO_2 dynamics that occurred in response to a stepwise change in the CO_2 partial pressure in the gas sparger. Furthermore, the model was used to predict CO_2 dynamics in photobioreactors with unicellular, nitrogen-fixing cyanobacterium *Cyanothece* sp. The metabolism changes dramatically during a day, and the distribution of CO_2 is expected to exhibit a pronounced diurnal modulation that significantly deviates from chemical equilibrium.

Keywords Algae · Carbon dioxide · Cyanobacteria · Mathematical model · Photosynthesis

L. Nedbal (✉) · J. Červený
Institute of Systems Biology and Ecology ASCR,
Zámek 136, 37333 Nové Hrady, Czech Republic
e-mail: nedbal@greentech.cz

L. Nedbal · J. Červený
Photon Systems Instruments, Ltd., Koláčkova 39,
62100 Brno, Czech Republic

N. Keren · A. Kaplan
Department of Plants and Environmental Sciences,
The Hebrew University of Jerusalem, Jerusalem 91904, Israel

List of symbols

a_B	Specific gas–liquid interfacial bubble area (m^{-1})
h	Henry constant (m^3 Pa mol^{-1})
k	Rate of CO_2 hydration (s^{-1})
k_L	Liquid-phase mass transfer coefficient (m s^{-1})
l	Rate of HCO_3^- dehydration (s^{-1})
n_{CO_2}	Number of CO_2 molecules (mol)
r_B	Bubble radius (m)
J	Aeration rate (m^3 s^{-1})
N_B	Number of bubbles
$P_{CO_2}^{bubble}$	Partial CO_2 pressure inside bubble (Pa)
$P_{CO_2}^{IN}$	Partial CO_2 pressure of gas entering bioreactor (Pa)
$P_{CO_2}^{OUT}$	Partial CO_2 pressure of gas leaving bioreactor headspace (Pa)
$P_{CO_2}^{X}$	Partial CO_2 pressure of bubble entering bioreactor headspace (Pa)
R	Universal gas constant (m^3 Pa K^{-1} mol^{-1})
S_B	Bubble surface (m^2)
S_H	Liquid to headspace surface (m^2)
T	Temperature of the photobioreactor (K)
V_B	Volume of bubble (m^3)
V_H	Volume of headspace (m^3)
V_L	Volume of liquid (m^3)
α_{CO_2}	Mass transfer rate from bubble to liquid phase (mol s^{-1})
β_{CO_2}	Mass transfer rate from headspace to liquid phase (mol s^{-1})

γ_{dCO_2}	Rate of dissolved carbon dioxide uptake by algae (mol s^{-1})
$\gamma_{HCO_3^-}$	Rate of bicarbonate uptake by algae (mol s^{-1})
τ	Bubble lifetime (s)
A	Flux of CO_2 into bioreactor (mol s^{-1})
B	Flux of CO_2 into headspace (mol s^{-1})
Γ	Flux of CO_2 out of bioreactor (mol s^{-1})
$[dCO_2]$	Concentration of CO_2 dissolved in liquid phase (mol m^{-3})
$[HCO_3^-]$	Concentration of bicarbonate ions in liquid phase (mol m^{-3})

Introduction

It is of immense importance to develop carbon-neutral or even carbon-capturing technologies that may mitigate the dynamics of the climatic implications of rising anthropogenic CO_2 emissions [6]. To operate on the scale of natural carbon cycle pools [11], one has to consider processes of proportional capacity such as photosynthesis, which has played the decisive role in stabilizing the global ecosystem within the present limits for billions of years [12]. Today, photosynthesis also promises production of third-generation biofuels that may assist in recycling atmospheric CO_2 [1, 4]. Photosynthetic microorganisms are also considered for biomineralization by point-source carbon capture [8, 20]. In another representation of biological carbon capture, CO_2 is an important substrate for intensive culturing of microalgae [5, 18]. CO_2-enriched air used for sparging was shown to enhance the productivity of microalgae under both laboratory and industrial mass culture conditions [1, 25, 30].

Among the processes that need to be better understood is the mass transfer of CO_2 between the gaseous and liquid phases of algal culture systems as well as the dynamics of dissolved inorganic carbon (Ci) that is, typically, in the form of aqueous dissolved CO_2 (dCO_2) or bicarbonate ion (HCO_3^-). The capacity of the particular organism to utilize preferably either dCO_2 or HCO_3^- is species dependent [7, 9, 19]. Furthermore, massive biological cycling of Ci has been demonstrated in representatives of the main algal groups [27]. Some algae take up CO_2 from the medium and release HCO_3^-, whereas others transport HCO_3^- inward and release excess CO_2. In some cases, the cycling may reach values 7 times larger than the rate of net photosynthesis [26]. Cycling of Ci constitutes part of the CO_2 concentrating mechanism [7, 9, 16] shown to raise the CO_2 concentration in close proximity to the universal carboxylating enzyme, ribulose 1,5-bisphosphate carboxylase/oxygenase (Rubisco) in most algal systems examined to date [19].

Thus, one needs to understand the entire system from gas sparging in the algal units to biological assimilation and cycling. To address these challenges, we developed and herein present a mathematical model of CO_2 mass transfer dynamics in a flat-panel algal photobioreactor [2, 15]. Model parameters allow simulation of different scenarios that may be relevant in industrial applications. The model is validated in a set of technical and biological experiments.

Materials and methods

Culture conditions

The unicellular nitrogen-fixing cyanobacterium *Cyanothece* sp. ATCC 51142 [13, 21, 23] was cultured in artificial ASP2 seawater medium [17] as modified [29] without nitrate. The pH of the medium was buffered at pH 7.5 using 17 mM TAPS biological buffer, and temperature was stabilized at 30 ± 0.2°C. For a detailed description of experimental protocols see [3].

Photobioreactor

The growth chamber of the temperature-controlled bioreactor unit (FMT-150, Photon Systems Instruments, Brno, Czech Republic) consists of a parallel-plate glass cuvette (20 cm × 10.1 cm × 6 cm) filled with 1,200 ml liquid media or algal suspension depending on experiment setup (see "Liquid media for the technical experiments" section for more details). The capabilities of the bioreactor were expanded by including gas-mixing and gas-analyzing utilities, and by incorporation of electrodes for measuring levels of CO_2 and O_2 dissolved in the suspension [2]. Specific gas mixture was dispersed into seven bubble streams by orifices in a stainless-steel tube at the bottom of the bioreactor cuvette. Other construction details of the instrument have been described previously [15].

Gas composition and flow rate control

A mass flow control system (GMS-150; Photon Systems Instruments, Brno, Czech Republic), was used to stabilize the composition of the CO_2-enriched gas supply. The gas flow through the photobioreactor was measured by MASS-VIEW (Bronkhorst High-Tech BV, Ruurlo, The Netherlands) and controlled by a high-precision valve (Parker Hannifin, Cleveland, USA). The composition of the exhaust gas escaping from the photobioreactor was monitored by an infrared CO_2 gas analyzer (Vaisala, Helsinki, Finland).

Liquid media for the technical experiments

The model was validated using media of pH 4.0 and pH 7.4, in which the CO_2 appears dominantly as dCO_2 and HCO_3^-, respectively. The pH 4.0 medium was prepared from deionized H_2O by adding 30 ml acetic buffer solution (0.1 M acetic acid, 0.02 M NaOH, adjusted to pH 4.0). The pH 7.4 medium was prepared by using TAPS biological buffer (17 mM, [(2-hydroxy-1,1-bis(hydroxymethyl)ethyl) amino]-1-propanesulfonic acid; Sigma, St. Louis, USA). Long-term pH stability was continuously monitored during the experiments and maintained by drops of 0.2 M NaOH when needed.

Results and discussion

Model

The scheme in Fig. 1 shows the model compartments, components, and parameters. For simplicity, we assume that both the liquid and the gaseous headspace are perfectly mixed, leading to uniform molar concentrations and partial pressures within the respective compartments. The CO_2 partial pressure in a bubble of CO_2-enriched air is high at the bottom of the photobioreactor and gradually decreases by mass transfer to the liquid while the bubble travels upward. The dynamics of the CO_2 partial pressure inside the bubble is described by $P^{\text{bubble}}_{CO_2(t)}$, where t is the time between the bubble leaving the sparging tube at $t = 0$ s $\left(P^{\text{bubble}}_{CO_2(t=0\,\text{s})} = P^{\text{IN}}_{CO_2}\right)$ and $t = \tau$ s when emerging into the headspace $\left(P^{\text{bubble}}_{CO_2(t=\tau)} \approx P^{X}_{CO_2}\right)$. Using Henry's law, the mass transfer rate between the bubble and the liquid phase can be calculated using Eq. (1):

$$\frac{\Delta\,\text{number of CO}_2\text{ moles transferred to water}}{\Delta\text{time}} \equiv \frac{\Delta n_{CO_2}}{\Delta t} = k_L S_B\left(\frac{P^{\text{bubble}}_{CO_2(t)}}{h} - [dCO_2]_{(t)}\right), \quad (1)$$

where k_L is the mass transfer coefficient, S_B is the surface of the bubble ($\sim 4\pi r_B^2$, where r_B is the effective bubble radius), $P^{\text{bubble}}_{CO_2(t)}$ is the instantaneous CO_2 partial pressure in a bubble at time t, h is the Henry constant at temperature T, and $[dCO_2]$ is the concentration of CO_2 dissolved in the liquid phase. The mass transfer is, at the same time, changing the CO_2 partial pressure in the bubble:

$$\frac{\Delta\,\text{number of CO}_2\text{ moles lost by the bubble}}{\Delta\text{time}} \equiv \frac{\Delta n_{CO_2}}{\Delta t} = -\frac{V_B}{RT}\frac{dP^{\text{bubble}}_{CO_2(t)}}{dt}, \quad (2)$$

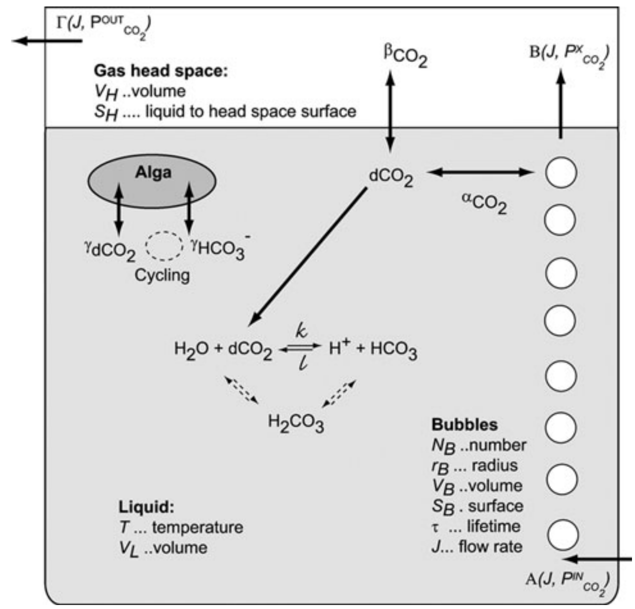

Fig. 1 Scheme of CO_2 mass transfer in a flat-panel algal photobioreactor. CO_2-enriched air enters the photobioreactor through a sparging tube, generating on average N_B bubbles of effective mean radius r_B (m). The average bubble lifetime is τ (s). The gaseous and liquid phases are assumed to be of the same temperature T (K). The volume of the liquid phase is V_L (m^3), and the surface between the liquid and the gaseous headspace is S_H (m^2). The headspace volume is V_H (m^3). The gas flow through the photobioreactor is constant at J ($m^3\,s^{-1}$), entering with CO_2 partial pressure of $P^{\text{IN}}_{CO_2}$ (Pa), so that the resulting CO_2 mass transfer flux into the photobioreactor is A (mol s^{-1}). The CO_2 partial pressure of the gas flow from bubbles to the headspace is $P^{X}_{CO_2}$ (Pa), resulting in CO_2 flux of B (mol s^{-1}). The CO_2 partial pressure in the headspace and in the exhaust gas is assumed to be uniform $P^{\text{OUT}}_{CO_2}$ (Pa), leading to residual CO_2 flux out of the photobioreactor of Γ (mol s^{-1}). The integral mass transfer flux of CO_2 from bubbles to the liquid medium is α_{CO_2} (mol s^{-1}), from the headspace to the liquid medium it is β_{CO_2} (mol s^{-1}), from the pool of dissolved CO_2 to algae it is γ_{dCO_2} (mol s^{-1}), and from the bicarbonate pool to the algae $\gamma_{HCO_3^-}$ (mol s^{-1}). The two latter rate constants, γ_{dCO_2} and $\gamma_{HCO_3^-}$, reflect also the extracellular biological cycling between the two forms. A more technical description and drawing of the photobioreactor have been published previously [15]

where V_B is the effective volume of the bubble ($\sim 4\pi r_B^2/3$) and R is the universal gas constant. The Eqs. 1 and 2 express the same quantity and, thus:

$$\frac{dP^{\text{bubble}}_{CO_2(t)}}{dt} = -k_L a_B RT\left(\frac{P^{\text{bubble}}_{CO_2(t)}}{h} - [dCO_2]_{(t)}\right), \quad (3)$$

where $a_B = S_B/V_B$.

The dynamics of the CO_2 partial pressure in a bubble can be calculated analytically assuming that the liquid volume is much larger than the bubble volume $V_L \gg V_B$ and, thus, the mass transfer from the single bubble changes the concentration of the dissolved CO_2 negligibly: $\frac{d}{dt}\left(\frac{P^{\text{bubble}}_{CO_2(t)}}{h}\right) \gg \frac{d}{dt}[dCO_2]_{(t)}$, i.e., $[dCO_2]$ is approximately constant during the lifetime of a bubble. Then, Eq. 3 can be approximated by

$$h\frac{\mathrm{d}}{\mathrm{d}t}\left(\frac{P^{\mathrm{bubble}}_{\mathrm{CO_2}(t)}}{h}-[\mathrm{dCO_2}]\right)=-k_{\mathrm{L}}a_{\mathrm{B}}RT\left(\frac{P^{\mathrm{bubble}}_{\mathrm{CO_2}(t)}}{h}-[\mathrm{dCO_2}]\right). \tag{4}$$

Using the initial condition $P^{\mathrm{bubble}}_{\mathrm{CO_2}(t=0\,s)}=P^{\mathrm{IN}}_{\mathrm{CO_2}}$, Eq. 4 can be solved to:

$$P^{\mathrm{bubble}}_{\mathrm{CO_2}(t)}=P^{\mathrm{IN}}_{\mathrm{CO_2}}\left[\exp\left(-\left(\frac{k_{\mathrm{L}}a_{\mathrm{B}}RT}{h}t\right)\right)\right]+h[\mathrm{dCO_2}]\left[1-\exp\left(-\left(\frac{k_{\mathrm{L}}a_{\mathrm{B}}RT}{h}t\right)\right)\right]. \tag{5}$$

Extending the calculation to a flow of N_{B} bubbles, Eq. 6 can be derived to quantify the mass transfer rate from the bubble flow to the liquid phase ($\alpha_{\mathrm{CO_2}}$ in Fig. 1):

$$\alpha_{\mathrm{CO_2}}=N_{\mathrm{B}}\frac{\Delta n_{\mathrm{CO_2}}}{\tau}=N_{\mathrm{B}}\frac{V_{\mathrm{B}}}{RT}\frac{P^{\mathrm{IN}}_{\mathrm{CO_2}}-P^{\mathrm{X}}_{\mathrm{CO_2}}}{\tau}=\frac{J}{RT}\left(P^{\mathrm{IN}}_{\mathrm{CO_2}}-P^{\mathrm{X}}_{\mathrm{CO_2}}\right), \tag{6}$$

where $P^{\mathrm{X}}_{\mathrm{CO_2}}=P^{\mathrm{bubble}}_{\mathrm{CO_2}(t=\tau)}$ is the CO_2 partial pressure of the gas entering the headspace from the bubble flow (Fig. 1), which can be calculated from Eq. 5 to yield

$$\alpha_{\mathrm{CO_2}}=\frac{J}{RT}\left\{P^{\mathrm{IN}}_{\mathrm{CO_2}}-h[\mathrm{dCO_2}]_{(t)}\right\}\left\{1-\exp\left[-\left(\frac{k_{\mathrm{L}}a_{\mathrm{B}}RT}{h}\tau\right)\right]\right\}. \tag{7}$$

The bubble stream brings into the headspace a flux of gas J of CO_2 partial pressure $P^{\mathrm{X}}_{\mathrm{CO_2}}=P^{\mathrm{bubble}}_{\mathrm{CO_2}(t=\tau)}$ that can also be calculated from Eq. 5. The corresponding mass transfer flux (Fig. 1) is

$$B(t)=\frac{J}{RT}\left\{P^{\mathrm{IN}}_{\mathrm{CO_2}}\exp\left(-\left(\frac{k_{\mathrm{L}}a_{\mathrm{B}}RT}{h}\tau\right)\right)+h[\mathrm{dCO_2}]_{(t)}\left[1-\exp\left(-\left(\frac{k_{\mathrm{L}}a_{\mathrm{B}}RT}{h}\tau\right)\right)\right]\right\}. \tag{8}$$

Another CO_2 mass transfer processes occur across the photobioreactor water surface from the headspace:

$$\beta(t)=-k_{\mathrm{L}}S_{\mathrm{H}}\left(\frac{P^{\mathrm{OUT}}_{\mathrm{CO_2}(t)}}{h}-[\mathrm{dCO_2}]_{(t)}\right), \tag{9}$$

and due to the gas leaving the headspace through the exhaust:

$$\Gamma(t)=-\frac{J}{RT}P^{\mathrm{OUT}}_{\mathrm{CO_2}(t)}. \tag{10}$$

The CO_2 partial pressure in the headspace and, thus, in the outgoing gas is determined by sum of the fluxes in and out of the headspace:

$$\frac{\mathrm{d}P^{\mathrm{OUT}}_{\mathrm{CO_2}(t)}}{\mathrm{d}t}=\frac{RT}{V_{\mathrm{H}}}[B(t)+\beta(t)+\Gamma(t)], \tag{11}$$

where V_{H} is the volume of the headspace. Equation 11 can be integrated numerically to reveal the dynamics of the CO_2 partial pressure in the headspace.

The CO_2 mass transfer processes of rate $\alpha_{\mathrm{CO_2}}$ from the bubble flow and $\beta_{\mathrm{CO_2}}$ from the headspace modify the concentration of the carbon dioxide dissolved in the liquid phase $[\mathrm{dCO_2}]$:

$$\frac{\mathrm{d}[\mathrm{dCO_2}]}{\mathrm{d}t}=\frac{J}{RT}\frac{h}{V_L}\left(\frac{P^{\mathrm{IN}}_{\mathrm{CO_2}}}{h}-[\mathrm{dCO_2}]_{(t)}\right)\times\left\{1-\exp\left[-\left(\frac{k_{\mathrm{L}}a_{\mathrm{B}}RT}{h}\tau\right)\right]\right\}-k_{\mathrm{L}}\frac{S_{\mathrm{H}}}{V_{\mathrm{L}}}\left(\frac{P^{\mathrm{OUT}}_{\mathrm{CO_2}(t)}}{h}-[\mathrm{dCO_2}]_{(t)}\right). \tag{12}$$

Using $P^{\mathrm{OUT}}_{\mathrm{CO_2}(t)}$ from the numerical integration of Eq. 11, Eq. 12 can also be integrated numerically to yield the dynamics of the dissolved CO_2 $[\mathrm{dCO_2}]$ at low pH (negligible reaction to bicarbonate) and in the absence of algae.

At neutral pH, the dissolved CO_2 can be hydrated to bicarbonate (Fig. 1). The alternative pathway involving carbonic acid (dashed arrows in Fig. 1) is integrated in form of effective rates of CO_2 hydration k and of HCO_3^- dehydration l as in [24]. The reactions involving bicarbonate are included in Eqs. 13 and 14:

$$\frac{\mathrm{d}[\mathrm{dCO_2}]_{(t)}}{\mathrm{d}t}=\frac{J}{RT}\frac{h}{V_{\mathrm{L}}}\left(\frac{P^{\mathrm{IN}}_{\mathrm{CO_2}}}{h}-[\mathrm{dCO_2}]_{(t)}\right)\times\left\{1-\exp\left[-\left(\frac{k_{\mathrm{L}}a_{\mathrm{B}}RT}{h}\tau\right)\right]\right\}-k_{\mathrm{L}}\frac{S_{\mathrm{H}}}{V_{\mathrm{L}}}\left(\frac{P^{\mathrm{OUT}}_{\mathrm{CO_2}(t)}}{h}-[\mathrm{dCO_2}]_{(t)}\right)+\ell\left[\mathrm{HCO_3^-}\right]_{(t)}-k[\mathrm{dCO_2}]_{(t)}-\gamma_{\mathrm{dCO_2}}, \tag{13}$$

$$\frac{\mathrm{d}\left[HCO_3^-\right]_{(t)}}{\mathrm{d}t}=k[\mathrm{dCO_2}]_{(t)}-\ell\left[\mathrm{HCO_3^-}\right]_{(t)}-\gamma_{\mathrm{HCO_3^-}}. \tag{14}$$

The rates $\gamma_{\mathrm{dCO_2}}$ and $\gamma_{\mathrm{HCO_3^-}}$ represent the uptake of dissolved carbon dioxide dCO_2 and of bicarbonate HCO_3^- by algae as well as the cycling between these forms [7, 9, 19].

Technical experiment

The dynamics of the CO_2 partial pressure in the exhaust of the bioreactor was measured during a transition caused by an abrupt change of the CO_2 partial pressure at the photobioreactor gas input (open circles in Fig. 2). The same dynamics were modeled as described above using Eq. 11 (thick solid lines in Fig. 2).

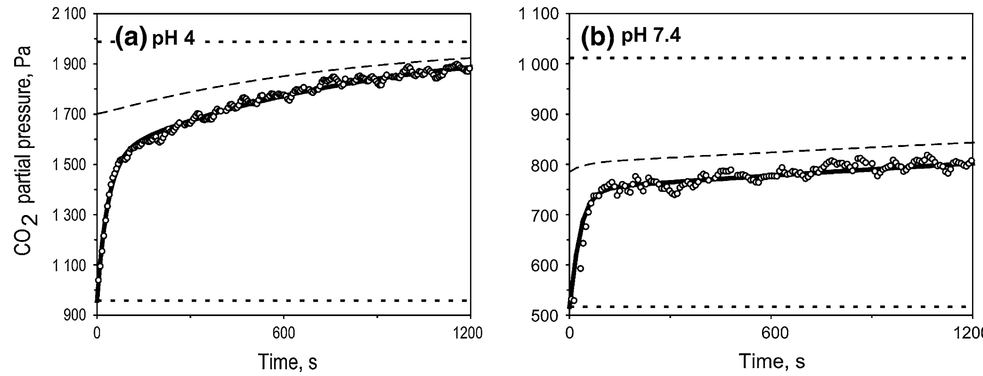

Fig. 2 Modeled and measured CO_2 partial pressure in the photobioreactor exhaust gas under different conditions. **a** pH 4.0, $T = 303$ K, at $t = 0$ s equilibrium with $P^{IN}_{CO_2} = 946$ Pa and $t > 0$ s $P^{IN}_{CO_2} = 1962$ Pa. **b** pH 7.4, $T = 303$ K, at $t = 0$ s equilibrium with $P^{IN}_{CO_2} = 510$ Pa and $t > 0$ s $P^{IN}_{CO_2} = 998$ Pa. *Dotted lines* indicate the starting ($t \leq 0$ s) and set ($t \geq 0$ s) CO_2 partial pressure at the input of the photobioreactor. *Open circles* show the measured CO_2 partial pressure in the photobioreactor exhaust, and *thick solid lines* under the *circles* show the model prediction. The *dashed line* shows the modeled CO_2 partial pressure in the bubbles at the time when they reach the water surface

The fixed parameters were: photobioreactor liquid volume $V_L = 1.2 \times 10^{-3}$ m^3 (1.2 l), liquid to headspace surface $S_H = 6.3 \times 10^{-3}$ m^2, gas flow rate 3.3×10^{-6} m^3 s^{-1} (200 ml min^{-1}), and mean number of bubbles $N_B \approx 400$ (counted from photographs). The bubble lifetime, the headspace volume, and the mass transfer coefficient were considered variable and found by using the Solver add-on to the Excel program (Microsoft Corp., USA) for the best fit between the data and the model.

The bubble lifetime was $\tau \approx 1.2$ s, and the mean bubble radius was $r_B \approx 1.3 \times 10^{-3}$ m. The headspace volume was $V_H \approx 158 \times 10^{-6}$ m^3 (158 ml) in the experiment with pH 4.0, and 172×10^{-6} m^3 (172 ml) with pH 7.4. The difference in head volumes is explained by evaporation of media during lengthy repetitions of the experiments.

The numerical fit for the mass transfer yielded a coefficient value of $k_L \approx 1.36 \times 10^{-4}$ m s^{-1} in the experiment with pH 4.0, and 1.78×10^{-4} m s^{-1} with pH 7.4.

Other fitted parameters in pH 7.4 were the effective rate constants of CO_2 hydration ($k \approx 2.1 \times 10^{-2}$ s^{-1}) and of HCO_3^- dehydration ($l \approx 2.2 \times 10^{-3}$ s^{-1}). The model predictions also matched dynamics of dissolved CO_2 (not shown).

Modeling a biological experiment

The dynamics of the CO_2 distribution in algal photobioreactors is massively influenced by the metabolic activities. Figure 3 shows the dynamics of dissolved CO_2 (full circles) in a photobioreactor [2, 15] in which a culture of *Cyanothece* sp. ATCC 51142 was grown in 16 h light (solid line) and 8 h dark (grey columns). A homologous experiment was comprehensively described previously [3].

Upon illumination in the morning, the cyanobacteria lower the dissolved CO_2 concentration approximately in proportion to the incident irradiance. The maximum depression was reached in the early afternoon hours to $\sim$270 µM dCO_2 (labeled 1 in Fig. 3). This is where the maximal combined photosynthetic and Ci cycling rate are reached in the culture. Later in the afternoon, the metabolic transition from fast photosynthesis and Ci cycling to strong respiration [3] and CO_2 release from the internal pool was manifested by the sharp increase of dCO_2 well above equilibrium to $\sim$410 µM dCO_2 (labeled 2 in Fig. 3). The prevailing respiration can be modeled by negative values of the rate γ_{dCO_2} in Eq. 13. The dusk respiratory peak is very

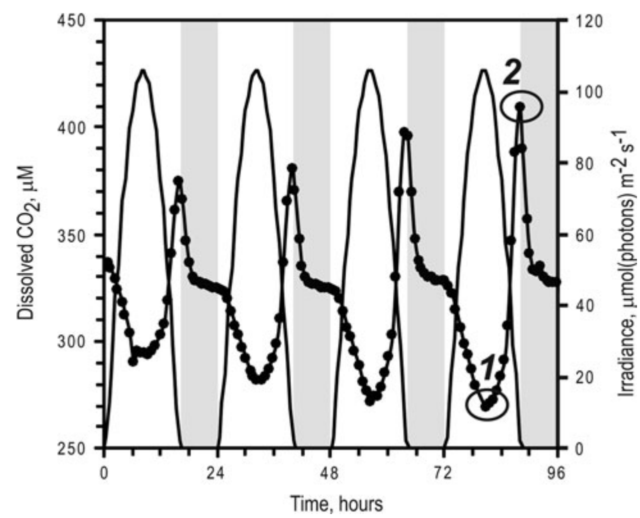

Fig. 3 Concentration of dissolved CO_2 (*closed circles*) in a photobioreactor described in Ref. [15]. The diurnal modulation of dissolved CO_2 was caused by intense metabolic activity of the cyanobacterium *Cyanothece* sp. ATCC 51142 grown in the photobioreactor. Temperature was 30°C, pH was stabilized at 7.5, and the flow of CO_2-enriched air was 200 ml min^{-1}. The CO_2 concentration at the photobioreactor input was 11,000 ppm ($\sim$1,115 Pa). Other details of the experimental materials and methods were as in Ref. [3]

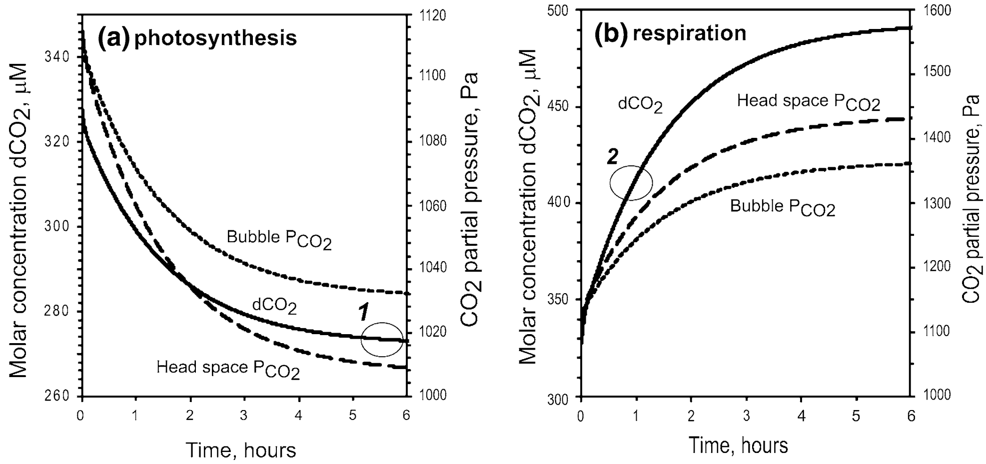

Fig. 4 Dynamics of dissolved CO_2 (*solid line*) calculated for cyanobacterial photosynthetic activity (**a**) of 70×10^{-3} mol(CO_2) mol(Chl)$^{-1}$ s^{-1} at culture density of 1.7 µM(Chl). The model parameters were as described above. The input partial pressure of CO_2 was as in Fig. 3 (~1,115 Pa). Photosynthetic activity was modeled as starting at $t = 0$ h. **b** Modeled effect of respiratory activity that was supposed to be 3 times higher than the photosynthetic activity in **a**. The *dotted* and *dashed lines* in both **a** and **b** show the calculated partial pressure of CO_2 in bubbles reaching the water surface and in the headspace, respectively

dynamic—its typical half-time period can be estimated by Fourier analysis of the transient at around 3.25 h, while the amplitude of the respective modulation was ~70 µM dCO_2.

Figure 4 documents that, solving numerically our model equations 13 and 14, one can show that cyanobacterial suspension corresponding to pigment density of 1.7×10^{-6} M(Chl) of typical photosynthetic and Ci cycling activity of 70×10^{-3} mol(CO_2) mol(Chl)$^{-1}$ s^{-1} [2, 10] can lower the dissolved CO_2 to ~270 µM dCO_2 (labeled 1 in Figs. 3 and 4a). The transition due to the gradually increasing photosynthetic CO_2 uptake (depression around midday in Fig. 3) is relatively slow and, thus, is not significantly limited by the CO_2 mass transfer between the gas and water in the photobioreactor. The sharp respiratory peak in the late afternoon hours is a dynamic feature that cannot be accounted for by a steady state. Figure 4b shows an attempt to model respiratory activity that could lead to a rapid (~1 h) increase to 410 µM dCO_2 (labeled 2 in Fig. 3). The respiration activity leading to this result was ~3 times higher than the photosynthetic activity estimated in Fig. 4a to elicit a sharp rise similar to that in Fig. 3 (label 2).

The capacity of the model to provide insights that would be difficult to measure experimentally is demonstrated by the calculated dynamics of the CO_2 partial pressure in the bubbles reaching the water surface (dotted lines in Fig. 4a, b). In contrast, the CO_2 partial pressure in the headspace (dashed lines in Fig. 4a, b) can be directly measured and used for future model validation.

Conclusions

The model presented herein offers insight into the dynamics of fluxes of different forms of CO_2 in an algal photobioreactor. The model fits experimental data measured during a transition between different levels of input partial pressure of CO_2 at pH 4.0 and pH 7.4. The fit was obtained with variable rate constants of dCO_2 hydration (k) and HCO_3^- dehydration (l). The best fit was obtained for $k \approx 2.1 \times 10^{-2}$ s^{-1} and $l \approx 2.2 \times 10^{-3}$ s^{-1}. These values are not far from earlier reported values [24] for pH 7.5 ($k \approx 4.0 \times 10^{-2}$ s^{-1} and $l \approx 3.5 \times 10^{-3}$ s^{-1}).

The model was further validated by explaining the midday depression in dissolved CO_2 concentration due to photosynthetic activity of cyanobacteria that agrees with typically measured rates. The most important conclusion of the paper is that the dissolved CO_2 and bicarbonate concentrations in the photobioreactor media can be displaced far from equilibrium by metabolic events, such as the dynamic respiratory peak of *Cyanothece* sp. that occurs in late afternoon hours of the diurnal cycle. Such dynamic events can dramatically affect the carbon balance of algal bioreactors in industrial applications. Also affected will be the energetic content of the produced biomass.

Model approximations and an outlook on further model improvement

Further refinement of the model is planned to account for diverse pH regimes. Namely, one may wish to model the frequent bioreactor regimes in which the suspension pH is automatically adjusted by bursts of CO_2 or with free-drifting pH, experimental modes described in detail previously [15, Figs. 6B or Fig. 6A]. Issues that should also be considered are real-life deviations from the present model assumptions. Namely, we assumed that diverse bubbles in the modeled photobioreactor volume can be represented by a uniform and constant effective size of bubbles with identical lifetime. In real flat-panel photobioreactors a uniform bubble lifetime is hard to achieve because of the statistical bubble radius dispersion and frequently uneven flow rates of bubbles along the horizontal photobioreactor profile. Also, we neglected the fact that the pressure in bubbles leaving the sparger tube is higher than in bubbles approaching the water surface. The effect on the bubble size of the CO_2 transfer during the bubble lifetime is on the other hand tiny, as the typical CO_2 concentrations are from 380 ppm to 20,000 ppm. Furthermore, the partial removal of CO_2 from the bubbles is compensated by O_2 uptake during the day, and vice versa at night. Among the issues that remain to be addressed are effects of salinity and ionic strength in the media [28, 31]. For that, integration with existing models [14, 22] will be pursued.

In spite of these limitations, we expect that the proposed improvements will be formulated as amendments of the model proposed here rather than its replacement.

Acknowledgments L.N. and J.Č. were supported by grants AV0Z60870520 (Czech Academy of Sciences), and by GAČR 206/09/1284 (Czech Science Foundation) as well as by Photon Systems Instruments, Ltd. N.K. and A.K. were supported by grants from the Israel Science Foundation (Bikura program) and the Hebrew University. The authors are grateful to Rainer Machne of Universität Wien for critically checking the model equations and reading of the manuscript.

References

1. Brennan L, Owende P (2010) Biofuels from microalgae—a review of technologies for production, processing, and extractions of biofuels and co-products. Renew Sustain Energy Rev 14(2):557–577. doi:10.1016/j.rser.2009.10.009
2. Červený J, Šetlík I, Trtílek M, Nedbal L (2009) Photobioreactor for cultivation and real-time, in situ measurement of O_2 and CO_2 exchange rates, growth dynamics, and of chlorophyll fluorescence emission of photoautotrophic microorganisms. Eng Life Sci 9(3):247–253. doi:10.1002/elsc.200800123
3. Červený J, Nedbal L (2009) Metabolic rhythms of the cyanobacterium *Cyanothece* sp. ATCC 51142 correlate with modeled dynamics of circadian clock. J Biol Rhythms 24(4):295–303. doi:10.1177/0748730409338367
4. Chisti Y (2008) Biodiesel from microalgae beats bioethanol. Trends Biotechnol 26(3):126–131. doi:10.1016/j.tibtech.2007.12.002
5. Chrismadha T, Borowitzka M (1994) Effect of cell density and irradiance on growth, proximate composition and eicosapentaenoic acid production of *Phaeodactylum tricornutum* grown in a tubular photobioreactor. J Appl Phycol 6(1):67–74. doi:10.1007/BF02185906
6. Falkowski P, Scholes RJ, Boyle E, Canadell J, Canfield D, Elser J, Gruber N, Hibbard K, Hogberg P, Linder S, Mackenzie FT, Moore B III, Pedersen T, Rosenthal Y, Seitzinger S, Smetacek V, Steffen W (2000) The global carbon cycle: a test of our knowledge of earth as a system. Science 290(5490):291–296. doi:10.1126/science.290.5490.291
7. Giordano M, Beardall J, Raven JA (2005) CO_2 concentrating mechanisms in algae: mechanisms, environmental modulation, and evolution. Annu Rev Plant Biol 56:99–131. doi:10.1146/annurev.arplants.56.032604.144052
8. Jansson C, Northen T (2010) Calcifying cyanobacteria—the potential of biomineralization for carbon capture and storage. Curr Opin Biotechnol 21(3):365–371. doi:10.1016/j.copbio.2010.03.017
9. Kaplan A, Reinhold L (1999) CO_2 concentrating mechanisms in photosynthetic microorganisms. Annu Rev Plant Physiol Plant Mol Biol 50(1):539–570. doi:10.1146/annurev.arplant.50.1.539
10. Lafarga-De la Cruz F, Valenzuela-Espinoza E, Millan-Nunez R, Trees CC, Santamaria-del-Angel E, Nunez-Cebrero F (2006) Nutrient uptake, chlorophyll a and carbon fixation by Rhodomonas sp. (Cryptophyceae) cultured at different irradiance and nutrient concentrations. Aquacult Eng 35(1):51–60. doi:10.1016/j.aquaeng.2005.08.004
11. Lal R (2008) Carbon sequestration. Philos Trans R Soc B Biol Sci 363(1492):815–830. doi:10.1098/rstb.2007.2185
12. Liu Z, Dreybrodt W, Wang H (2010) A new direction in effective accounting for the atmospheric CO_2 budget: Considering the combined action of carbonate dissolution, the global water cycle and photosynthetic uptake of DIC by aquatic organisms. Earth Sci Rev 99(3–4):162–172. doi:10.1016/j.earscirev.2010.03.001
13. Meunier PC, Colon-Lopez MS, Sherman LA (1998) Photosystem II cyclic heterogeneity and photoactivation in the diazotrophic, unicellular cyanobacterium *Cyanothece* species ATCC 51142. Plant Physiol 116(4):1551–1562
14. Millero FJ, Graham TB, Huang F, Bustos-Serrano H, Pierrot D (2006) Dissociation constants of carbonic acid in seawater as a function of salinity and temperature. Mar Chem 100(1–2):80–94. doi:10.1016/j.marchem.2005.12.001
15. Nedbal L, Trtílek M, Červený J, Komárek O, Pakrasi HB (2008) A photobioreactor system for precision cultivation of photoautotrophic microorganisms and for high-content analysis of suspension dynamics. Biotechnol Bioeng 100(5):902–910. doi:10.1002/bit.21833
16. Price GD, Badger MR, Woodger FJ, Long BM (2007) Advances in understanding the cyanobacterial CO_2-concentrating-mechanism (CCM): functional components, Ci transporters, diversity, genetic regulation and prospects for engineering into plants. J Exp Bot. doi:10.1093/jxb/erm112
17. Provasoli L, McLaughlin JJA, Droop MR (1957) The development of artificial media for marine algae. Arch Mikrobiol 25(4):392–428
18. Raghavan G, Haridevi CK, Gopinathan CP (2008) Growth and proximate composition of the *Chaetoceros calcitrans* f. *pumilus* under different temperature, salinity and carbon dioxide levels. Aquacult Res 39(10):1053–1058. doi:10.1111/j.1365-2109.2008.01964.x
19. Raven JA, Cockell CS, De La Rocha CL (2008) The evolution of inorganic carbon concentrating mechanisms in photosynthesis. Philos Trans R Soc B Biol Sci 363(1504):2641–2650. doi:10.1098/rstb.2008.0020
20. Riding R (2009) An atmospheric stimulus for cyanobacterial-bioinduced calcification ca. 350 million years ago? Palaios 24(10):685–696. doi:10.2110/palo.2009.p09-033r
21. Schneegurt MA, Sherman DM, Sherman LA (1997) Growth, physiology, and ultrastructure of a diazotrophic cyanobacterium, *Cyanothece* sp. strain ATCC 51142, in mixotrophic and chemoheterotrophic cultures. J Phycol 33(4):632–642. doi:10.1111/j.1529-8817.1997.tb03958.x
22. Schulz KG, Riebesell U, Rost B, Thoms S, Zeebe RE (2006) Determination of the rate constants for the carbon dioxide to bicarbonate inter-conversion in pH-buffered seawater systems. Mar Chem 100(1–2):53–65. doi:10.1016/j.marchem.2005.11.001
23. Sherman LA, Meunier P, Colon-Lopez MS (1998) Diurnal rhythms in metabolism: a day in the life of a unicellular, diazotrophic cyanobacterium. Photosynth Res 58(1):25–42. doi:10.1023/A:1006137605802

24. Spalding MH, Portis AR (1985) A model of carbon dioxide assimilation in *Chlamydomonas reinhardii*. Planta 164(3): 308–320. doi:10.1007/BF00402942
25. Stephens E, Ross IL, King Z, Mussgnug JH, Kruse O, Posten C, Borowitzka MA, Hankamer B (2010) An economic and technical evaluation of microalgal biofuels. Nat Biotechnol 28(2):126–128. doi:10.1038/nbt0210-126
26. Tchernov D, Hassidim M, Luz B, Sukenik A, Reinhold L, Kaplan A (1997) Sustained net CO_2 evolution during photosynthesis by marine microorganism. Curr Biol 7(10):723–728. doi:10.1016/s0960-9822(06)00330-7
27. Tchernov D, Silverman J, Luz B, Reinhold L, Kaplan A (2003) Massive light-dependent cycling of inorganic carbon between oxygenic photosynthetic microorganisms and their surroundings. Photosynth Res 77(2):95–103. doi:10.1023/A:1025869600935
28. Tyrrell T, Zeebe RE (2004) History of carbonate ion concentration over the last 100 million years. Geochim Cosmochim Acta 68(17):3521–3530. doi:10.1016/j.gca.2004.02.018
29. van Baalen C (1962) Studies on marine blue-green algae. Bot Mar 4:129–139
30. Wang B, Li Y, Wu N, Lan C (2008) CO_2 bio-mitigation using microalgae. Appl Microbiol Biotechnol 79(5):707–718. doi:10.1007/s00253-008-1518-y
31. Zeebe RE, Wolf-Gladrow D (2001) Equilibrium. In: Zeebe RE, Wolf-Gladrow D (eds) CO_2 in seawater. Elsevier, Amsterdam, pp 1–84